A Robust Data-driven Controller Design Methodology for Particle Accelerator Power Converters

Achille Nicoletti, Michele Martino and Alireza Karimi

***Abstract*—A new data-driven approach using the frequency response function (FRF) of a system is proposed for designing robust H_∞ digital controllers for particle accelerators' power converters. This design method ensures that the dynamics of a system are captured and avoids the problem of unmodeled dynamics associated with parametric models. The H_∞ robust performance condition can be represented by a set of convex constraints with respect to the parameters of a two-degree of freedom RST controller. This controller is robust with respect to the frequency-dependent uncertainties of the frequency response function. Moreover, constraints will be imposed in order to simultaneously ensure the desired stability margins and the controller stability. A convex optimization algorithm is then implemented to obtain the controller parameters. The effectiveness of the method is illustrated by designing the controller for the Q-STRIP magnet power converter of the PS Booster accelerator upgrade project at CERN. Experimental validation in the time domain is also presented.**

***Index Terms*—Convex optimization, data-driven control, H-infinity, power converter control, robust control, RST**

I. Introduction

MANY of today's complex systems possess a multitude of uncertainties, and obtaining an accurate parametric model for such systems can be both laborious and impractical for controller synthesis. In industrial schemes, the dynamics of plants are typically approximated by low-order models, since the controller synthesis is easier to implement for lower order processes. However, this approximation can impede the performance of a controller, since low-order models are subject to model uncertainty. A survey on the differences associated with model-based control and data-driven control has been addressed in [1] and [2]; the authors assert that model-based control methods are inherently less robust due to the unmodeled dynamics of a process, and that these controllers are unsafe for practical applications. With the data-driven control scheme, the parametric uncertainties and the unmodeled dynamics are irrelevant and the only source of uncertainty is the measurement noise.

Data-driven controllers can be synthesized either on-line or off-line; the on-line methods such as the classical direct adaptive control (MRAC) [3], model-free adaptive control (MFAC) [4], and the unfalsified control (UC) [5] methodologies design controllers using time-domain data. Iterative feedback tuning (IFT) [6], correlation-based tuning (CBT) [7], virtual reference feedback tuning (VRFT) [8], non-iterative data-driven model reference control [9] methodologies are all off-line time-domain data-driven methods. The widely used PID controller is usually tuned based on a set of time-domain or frequency-domain data.

Data-driven control methods using frequency-domain data are design schemes that continue to spark the interest of many researchers. The frequency-domain approach offers many advantages compared to time-domain methods :

- Without knowledge of the transfer function, the dynamics of a system can be captured experimentally through the frequency response.
- Relative and absolute stability of a closed-loop system can be determined with the knowledge of the open-loop frequency response.
- Noise disturbance generated in the system can be easily determined using frequency analysis.
- System uncertainties can be modeled at discrete frequency points (which reduces the conservatism associated with uncertainty modeling).

The authors in [10] use the frequency response data of a stable system to design an optimal controller through a symmetric root locus technique. A robust frequency-domain control design method has been established in [11]; this method, however, requires a solution to a non-linear optimization problem. A frequency-domain loop-shaping approach to design fixed-structure controllers is presented in [12]. In this method, a convex optimization problem can be formulated if a linearly parameterized controller is considered; however, in this method, the closed-loop stability is not guaranteed and should be verified a posteriori. Robust controller design methods belonging to the $\mathcal{H}_\infty$ control framework minimizes the $\mathcal{H}_\infty$ norm of a weighted closed-loop sensitivity functions. In [13] a frequency-response method is proposed based on the Q-parametrization to guarantee the $\mathcal{H}_\infty$ performance for fixed-structure controllers. In [14], a frequency domain approach is realized where a convex optimization algorithm is formulated by considering a convex approximation of the $\mathcal{H}_\infty$ criterion. In order to obtain convexity, however, the controller is chosen to be linearly parameterized, i.e. the denominator of the controller are fixed. This limits the number of degrees of freedom of the controller, and thus impedes the controller performance. A frequency-domain approach for computing low-order multivariable linearly parameterized controllers is presented in [15]. The $\mathcal{H}_\infty$ constraints are convexified around an initial stabilizing controller. An iterative algorithm is used

Achille Nicoletti is with the Technology Department at European Organization for Nuclear Research (CERN) and the Automatic Control Laboratory at Ecole Polytechnique Fédérale de Lausanne (EPFL) (email: achille.nicoletti@cern.ch)

Michele Martino is with the Technology Department at European Organization for Nuclear Research (CERN) (email: michele.martino@cern.ch)

Alireza Karimi is with the Automatic Control Laboratory at Ecole Polytechnique Fédérale de Lausanne (EPFL) (email: alireza.karimi@epfl.ch)

that converges to a local optimal solution of the non-convex problem. The method in [14] is extended to data-driven gain-scheduled controller design in [16] and multivariable decoupling controller design in [17]. A public domain toolbox for Matlab is also available [18]. A similar approach is proposed in [19], where a convex-concave approximation of the $\mathcal{H}_\infty$ constraints based on an initial stabilizing controller is used. The extension of this method to design multivariable PID controllers for stable systems is presented in [20]. This method uses the same convex approximation as in [15] but is limited to stable systems and PID structure. The design of controllers that are not linear in parameters (e.g. represented by rational transfer functions) using frequency domain data are studied in [21]. The necessary and sufficient conditions for the existence of such controllers are developed. This method needs no initial stabilizing controller and converges to the optimal $\mathcal{H}_\infty$ performance when the order of the controller goes to infinity.

The RST controller structure is an effective discrete-time two-degree of freedom (2DOF) polynomial controller where the tracking and regulation characteristics of a closed-loop system can be formulated independently [22]. The RST controller design methodology is usually based on the pole placement technique and uses the dynamic model of the physical system. In [23], the data-driven frequency-domain approach of [14] is extended to RST controller design. However, in order to preserve convexity, this method requires one of the controller terms to be fixed a priori. This problem is fixed in [24], where an RST controller is designed in the $\mathcal{H}_\infty$ framework by formulating a convex optimization problem in a data-driven setting. The necessary and sufficient conditions for the existence of RST controllers that satisfy the $\mathcal{H}_\infty$ constraint only on one sensitivity function are also developed.

The proposed method in this paper is an extension of [24], where the necessary and sufficient conditions that ensures the $\mathcal{H}_\infty$ performance for multiple weighted sensitivity functions is presented. Moreover, the frequency-dependent uncertainties originated from the measurement noise are taken into consideration for robust performance specifications. Additionally, since the parameters of the controller's denominator are the optimization variables, this method can lead to unstable controllers. Therefore, a sufficient condition is presented to ensure that the controller remains stable. The proposed method is then used to design a robust RST controller for power converters in particle accelerators at CERN. The designed controller is implemented in the power converters to control their output current with extremely high precision. The main advantage of the proposed method for this application is to guarantee the robustness margins, high bandwidth and small tracking error by a data-driven convex optimization based approach that does not require the manual tuning of the classical pole-placement model-based approach.

The paper is organized as follows. The class of models, controllers and control objectives are defined in section (II). Section (III) discusses the control design methodology and stability conditions of the proposed method for the RST controller structure. Convex conditions are formulated based on the $\mathcal{H}_\infty$ criterion. Section (IV) discusses the framework of the power converter control system and its functionality at CERN. Section (V) is dedicated to a case study where the effectiveness of the method is demonstrated by applying the proposed design scheme to a power converter control system for a specific accelerator requirement. Finally, the concluding remarks are given in section (VI).

II. Problem Formulation

A. Preliminaries

Let $u[k]$ and $y[k]$ represent the input and output signals of a causal discrete-time system, respectively, where k is a discrete-time instant and T_s is the sampling period. Suppose that these signals are noise-free and have zero initial and final conditions (i.e., $u[k] = y[k] = 0$ for $k \leq 0$ and $k > K_s$). Then, the frequency response function (FRF) of the system can be represented as

$$G(e^{-j\omega}) = Y(e^{-j\omega})U^{-1}(e^{-j\omega}) \tag{1}$$

where

$$U(e^{-j\omega}) = \frac{1}{\sqrt{K_s}} \sum_{k=0}^{K_s} u[k]e^{-j\omega T_s k} \tag{2}$$

$$Y(e^{-j\omega}) = \frac{1}{\sqrt{K_s}} \sum_{k=0}^{K_s} y[k]e^{-j\omega T_s k} \tag{3}$$

are the periodograms of the input and output signals and $\omega \in [-\pi/T_s, \pi/T_s]$. Note that due to the symmetry of the periodograms, it is sufficient to consider $\omega \in [0, \pi/T_s]$ for practical applications. Under these assumptions, it is evident that from a set of sampled time-domain data, one is able to obtain a continuous FRF. If the data is noisy, then $G(e^{-j\omega})$ is characterized as the Empirical Transfer Function Estimate (ETFE) and is asymptotically unbiased [25]. For such systems, a multiplicative uncertainty can be considered to ensure robustness in the presence of noise perturbations.

Let the set $\mathscr{P}$ represent the family of all stable, proper, real-rational discrete-time transfer functions with no pole on the unit circle. It is imperative to note that $\mathscr{P}$ is closed under multiplication and addition; in other words, if $P_1(z^{-1}), P_2(z^{-1}) \in \mathscr{P}$, then

$$\{P_1(z^{-1}) + P_2(z^{-1}), P_1(z^{-1})P_2(z^{-1})\} \in \mathscr{P} \tag{4}$$

Suppose that a single-input-single-output (SISO) feedback control system structure is used where the plant is represented as $G(z^{-1}) = N(z^{-1})M^{-1}(z^{-1})$ such that $\{N(z^{-1}), M(z^{-1})\} \in \mathscr{P}$. As asserted in [26] and [27], if $\{N(z^{-1}), M(z^{-1})\} \in \mathscr{P}$, then $G(z^{-1}) = N(z^{-1})M^{-1}(z^{-1})$ is called a *coprime factorization* of $G(z^{-1})$ over $\mathscr{P}$.

B. Class of models

Let the FRF of such a factorized discrete-time SISO plant be defined as follows:

$$G(e^{-j\omega}) = N(e^{-j\omega})M^{-1}(e^{-j\omega}), \qquad \forall \omega \in \Omega \tag{5}$$

where $\Omega \in [0, \pi/T_s]$. $N(e^{-j\omega})$ and $M(e^{-j\omega})$ must be FRF's of bounded analytic functions outside the unit circle; for a stable plant, a trivial choice is $N(e^{-j\omega}) = G(e^{-j\omega})$ and

$M(e^{-j\omega}) = 1$. A discussion on how to formulate $N(e^{-j\omega})$ and $M(e^{-j\omega})$ for unstable processes can be found in [21]. In general, a set $\mathcal{G}$ can be formulated to represent a plant model containing p FRF models:

$$\mathcal{G} = \{G_l(e^{-j\omega}); \quad l = 1, \ldots, p; \quad \forall \omega \in \Omega\} \tag{6}$$

These FRF's can be determined by considering the frequency response of a parametric model or from a set of input/output data. For simplicity, one model from the set $\mathcal{G}$ will be considered, and the subscript l will be omitted. However, in general, the design procedures outlined in this paper can be applied to the multi-model case.

C. Frequency-domain uncertainty

Suppose that the uncertainty associated with a given FRF is described by an additive uncertainty:

$$\begin{aligned} \hat{N}(e^{-j\omega}) &= N(e^{-j\omega}) + |W_n(e^{-j\omega})|\delta_n e^{j\theta_n} \\ \hat{M}(e^{-j\omega}) &= M(e^{-j\omega}) + |W_m(e^{-j\omega})|\delta_m e^{j\theta_m} \end{aligned} \tag{7}$$

where $|\delta_n| \leq 1$, $|\delta_m| \leq 1$; $\{\theta_n, \theta_m\} \in [0, 2\pi]$; W_n and W_m are the uncertainty weighting filters which can be determined from the covariance of the estimates for a given confidence interval. As previously stated, $N(e^{-j\omega}) = G(e^{-j\omega})$ and $M(e^{-j\omega}) = 1$ can be selected for stable systems. Therefore, given the periodogram of G, the estimates of the real and the imaginary part of $N(e^{-j\omega})$ can be formulated; these estimates are asymptotically uncorrelated and normally distributed with a variance of $\Phi_v(\omega)/2|U(e^{-j\omega})|^2$, where $\Phi_v(\omega)$ is the spectrum of the disturbance $v[k]$ at the output of the plant ([25]). The additive uncertainty can be described in the complex plane with a disk centered at $N(e^{-j\omega})$ having a radius of $|W_n(e^{-j\omega})|$. The uncertainty is characterized by the Rayleigh distribution and can be determined for any probability level. For example, if it is desired to construct an uncertainty disk such that the true frequency response lies within the disk with a probability level of 0.95, then the radius of this disk will be

$$|W_n(e^{-j\omega})| = \sqrt{\frac{5.99\Phi_v(\omega)}{2|U(e^{-j\omega})|^2}} \tag{8}$$

The output noise spectrum can be estimated as

$$\Phi_v(\omega) = \Phi_y(\omega) - \frac{|\Phi_{uy}(\omega)|^2}{\Phi_u(\omega)} \tag{9}$$

where $\Phi_u(\omega)$ is the input spectrum, $\Phi_y(\omega)$ is the output spectrum, and $\Phi_{uy}(\omega)$ is the cross-spectral density of the input and output channels.

D. Class of controllers

The controller structure that will be considered will be of the RST-type. The RST controller is a two-degree of freedom controller which can be used to synthesize the tracking and regulation requirements independently from each other [22]. The general structure of this controller is shown in Fig. 1. Each controller is realized as a polynomial function as follows:

$$R(z^{-1}, \rho) = r_0 + r_1 z^{-1} + \cdots + r_{n_r} z^{-n_r} \tag{10}$$

$$S(z^{-1}, \rho) = 1 + s_1 z^{-1} + \cdots + s_{n_s} z^{-n_s} \tag{11}$$

$$T(z^{-1}, \rho) = t_0 + t_1 z^{-1} + \cdots + t_{n_t} z^{-n_t} \tag{12}$$

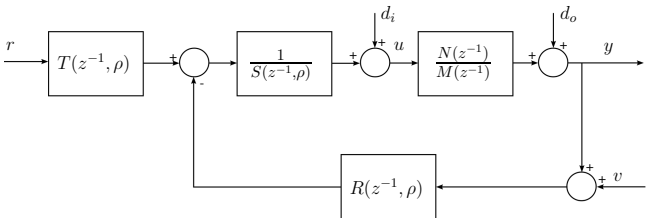

Fig. 1: RST controller structure

where $\{n_s, n_r, n_t\}$ are the orders of the polynomials R, S and T, respectively. These controllers can also be represented in a linear regression form as

$$\begin{aligned} R(z^{-1}, \rho) &= \rho_R^\top \phi_{n_r}(z^{-1}) = [r_0, r_1, \ldots, r_{n_r}]\phi_{n_r}(z^{-1}); \\ S(z^{-1}, \rho) &= \rho_S^\top \phi_{n_s}(z^{-1}) = [1, s_1, \ldots, s_{n_s}]\phi_{n_s}(z^{-1}); \\ T(z^{-1}, \rho) &= \rho_T^\top \phi_{n_t}(z^{-1}) = [t_0, t_1, \ldots, t_{n_t}]\phi_{n_t}(z^{-1}); \end{aligned}$$

where

$$\begin{aligned} \rho^\top &= [\rho_R^\top, \rho_S^\top, \rho_T^\top] \\ \phi_x^\top(z^{-1}) &= [1, z^{-1}, \ldots, z^{-x}] \end{aligned}$$

where $x \in \{n_r, n_s, n_t\}$.

Based on the internal model principle, the controller may contain the disturbance model to achieve a zero steady-state error. Therefore, the polynomials may be pre-multiplied with any arbitrary function that actualizes the desired action. For example, if it is desired to reject a step disturbance at the output, then $S(z^{-1}, \rho)$ can be pre-multiplied with $(1 - z^{-1})$ (which represents the integral action of the controller). For sinusoidal disturbances at specific frequencies, the polynomials can be pre-multiplied with the function

$$\theta(z^{-1}) = 1 - 2z^{-1}\cos(\omega_z T_s) + z^{-2}$$

where ω_z is the frequency in rad/s at which the disturbance occurs.

E. Sensitivity Functions

Since the design techniques introduced in this paper belong to the $\mathcal{H}_\infty$ framework, it is appropriate to consider the various sensitivity functions associated with the RST controller structure. Some sensitivity functions for this process can be asserted as follows:

$$\mathcal{S}_1(z^{-1}, \rho) = \frac{y}{d_o} = \frac{M(z^{-1})S(z^{-1}, \rho)}{\psi(z^{-1}, \rho)} \tag{13}$$

$$\mathcal{S}_2(z^{-1}, \rho) = \frac{y}{r} = \frac{N(z^{-1})T(z^{-1}, \rho)}{\psi(z^{-1}, \rho)} \tag{14}$$

$$\mathcal{S}_3(z^{-1}, \rho) = \frac{r - y}{r} = \frac{\psi(z^{-1}, \rho) - N(z^{-1})T(z^{-1}, \rho)}{\psi(z^{-1}, \rho)} \tag{15}$$

where $\psi(z^{-1}, \rho) = N(z^{-1})R(z^{-1}, \rho) + M(z^{-1})S(z^{-1}, \rho)$, y is the system output, r is the reference input, and d_o is the output disturbance. For notation purposes, the dependency in z^{-1} will be omitted, and will only be reiterated when deemed necessary. Note that all of the sensitivity functions are stable if the zeros of $\psi(\rho)$ lie within the unit circle. The sensitivity functions defined above (and all other sensitivity

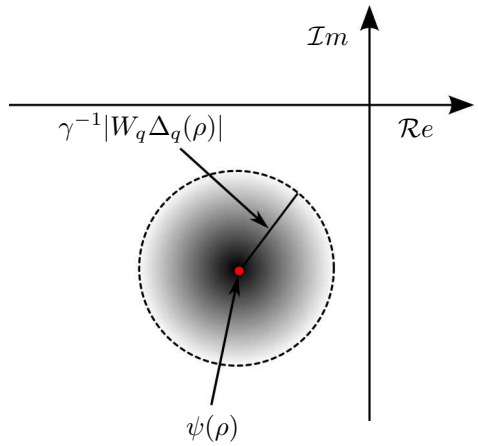

Fig. 2: The graphical interpretation of $\mathcal{H}_\infty$ constraints in the complex plane

functions of interest) all contain the same transfer function $\psi(\rho)$. Therefore, a general construction of the sensitivity function can be expressed as $\mathcal{S}_q(\rho) = \Delta_q(\rho)/\psi(\rho)$, where $\Delta_q(\rho)$ is a linear function of R, S and/or T. The subscript $q \in \{1, 2, \ldots, c\}$ denotes the q-th sensitivity of interest and c is the total number of sensitivity functions.

III. $\mathcal{H}_\infty$ Performance via Convex Optimization

A. General Design Specifications

In the general $\mathcal{H}_\infty$ control problem, the objective is to find the controller parameters vector ρ such that

$$\sup_{\omega\in\Omega} |H_q(e^{-j\omega}, \rho)| < \gamma \tag{16}$$

where $\gamma \in \mathbb{R}^+$, $H_q(e^{-j\omega}, \rho) = W_q(e^{-j\omega})\mathcal{S}_q(e^{-j\omega}, \rho)$ and W_q is the FRF of a stable weighting filter such that $H_q(e^{-j\omega}, \rho)$ has a bounded infinity norm. For notation purposes, the dependency in $e^{-j\omega}$ will be omitted, and will only be reiterated when deemed necessary. The condition in (16) can also be expressed as follows:

$$\gamma^{-1}|W_q\Delta_q(\rho)| < |\psi(\rho)|; \quad \forall\omega \in \Omega \tag{17}$$

It is desired to minimize the upper bound γ such that the $\mathcal{H}_\infty$ performance condition is satisfied. Therefore, the following optimization problem can be considered:

$$\begin{aligned} \underset{\rho}{\text{minimize}} \quad & \gamma \\ \text{subject to:} \quad & \gamma^{-1}|W_q\Delta_q(\rho)| < |\psi(\rho)| \\ & \forall\omega \in \Omega \quad ; \quad q \in \mathcal{Q} \subset \{1, 2, \ldots, c\} \end{aligned} \tag{18}$$

Notice that (18) is a non-convex optimization problem.

Consider a circle in the complex plane at a specific frequency in Ω which is centered at $\psi(\rho)$ and has radius $\gamma^{-1}|W_q\Delta_q(\rho)|$. The constraint in (17) ensures that for any frequency point in Ω, the circle associated with this frequency point will not encircle the origin. Fig. 2 displays the graphical interpretation of this condition. This geometrical construction will be used to prove the following Lemma:

Lemma 1. *Suppose that*

$$H_q(\rho, e^{-j\omega}) = W_q(e^{-j\omega})\Delta_q(\rho, e^{-j\omega})\psi^{-1}(\rho, e^{-j\omega})$$

is the frequency response of a bounded analytic function outside the unit circle. Then, the following constraint is met

$$\sup_{\omega\in\Omega} |H_q(\rho, e^{-j\omega})| < \gamma \tag{19}$$

if and only if there exists a finite-impulse-response (FIR) function $F(z^{-1})$ that satisfies

$$\Re\{\psi(\rho)F(e^{-j\omega})\} > \gamma^{-1}|W_q\Delta_q(\rho)F(e^{-j\omega})|, \qquad \forall\omega \in \Omega$$

Proof : The basic idea is similar to that of the proof of Theorem 1 in [28]. It is clear that (19) is satisfied if and only if the disk of radius $\gamma^{-1}|W_q\Delta_q(\rho)|$ centered at $\psi(\rho)$ does not include the origin for all $\omega \in \Omega$, i.e. $|\psi(\rho)| > \gamma^{-1}|W_q\Delta_q(\rho)|$. This is equivalent to the existence of a line passing through origin that does not intersect the disk. Therefore, at every given frequency, ω, there exists a complex number $f(e^{-j\omega})$ that can rotate the disk such that it lays inside the right hand side of the imaginary axis. Hence, we have

$$\begin{aligned} \Re\left\{\left[\psi(\rho) - \gamma^{-1}|W_q\Delta_q(\rho)|e^{j\theta}\right] f(e^{-j\omega})\right\} > 0 \\ \forall\omega \in \Omega, \forall\theta \in [0\,,\, 2\pi[\end{aligned} \tag{20}$$

where $\Re\{\cdot\}$ denotes the real part of a complex variable. Since $f(e^{-j\omega}) = |f(e^{-j\omega})|e^{j\theta_f}$, then the above condition can be expressed as

$$\begin{aligned} \Re\{\psi(\rho)f(e^{-j\omega})\} > \gamma^{-1}|W_q\Delta_q(\rho)f(e^{-j\omega})|\cos(\theta + \theta_f) \\ \forall\omega \in \Omega, \forall\theta \in [0\,,\, 2\pi[\end{aligned} \tag{21}$$

However, (21) is satisfied if and only if:

$$\begin{aligned} \Re\{\psi(\rho)f(e^{-j\omega})\} > \gamma^{-1}|W_q\Delta_q(\rho)f(e^{-j\omega})| \\ \forall\omega \in \Omega \end{aligned} \tag{22}$$

In [28], it is shown that, $f(e^{-j\omega})$ can be approximated arbitrarily well by the frequency response of a stable transfer function or FIR function $F(z^{-1})$ if and only if

$$Z = \left(\psi(\rho) - \gamma_0^{-1}|W_q\Delta_q(\rho)|e^{j\theta}\right)^{-1} \tag{23}$$

is analytic in the right half plane for all $\gamma_0 > \gamma$ and all $\theta \in [0\,,\, 2\pi[$. However, $\psi^{-1}(\rho)$ is stable because of the stability of $H_q(\rho)$. On the other hand, by decreasing γ_0 from infinity to γ, the poles of Z move continuously with γ_0. Therefore, Z is not analytic in the right half plane if and only if $Z^{-1}(e^{-j\omega}) = 0$ for a given frequency, which is not the case because the origin is not in the interior of the circle $\gamma_0^{-1}|W_q\Delta_q(\rho)|e^{j\theta}$. ■

The set of all controllers that meet the performance condition defined by the weighted norm of sensitivity functions is asserted in the following theorem.

Theorem 1. *Given the frequency response function $G(e^{-j\omega}) = N(e^{-j\omega})M^{-1}(e^{-j\omega})$ and the frequency response of a weighting filter $W_q(e^{-j\omega})$, then the following statements are equivalent for a given $q \in \mathcal{Q}$:*

(a) *There exists an RST controller that stabilizes G and*

$$\sup_{\omega\in\Omega} |W_q\mathcal{S}_q(\rho)| < \gamma \tag{24}$$

(b) *There exists an RST controller such that*

$$\Re\{\psi(\rho)\} > \gamma^{-1}|W_q\Delta_q(\rho)| \quad \forall\omega \in \Omega \tag{25}$$

Proof : (**b** $\Rightarrow$ **a**) $\psi(\rho)$ is analytic outside the unit circle and its real part is positive for all $\omega \in \Omega$. Therefore, $\psi(\rho)$ will not encircle the origin when ω travels along the Nyquist contour, and its inverse is stable. This implies that $R(\rho)$ and $S(\rho)$ stabilizes G. On the other hand, we have

$$|\psi(\rho)| \geq \Re\{\psi(\rho)\} \quad \forall\omega \in \Omega$$

which leads to

$$|W_q\Delta_q(\rho)| < \gamma|\psi(\rho)| \quad \forall\omega \in \Omega \tag{26}$$

Therefore, (26) leads to (24) in Statement (**a**).

(**a** $\Rightarrow$ **b**) Assume that $R(\rho_0)$, $S(\rho_0)$, and/or[1] $T(\rho_0)$ satisfies Statement (**a**) but not Statement (**b**). Then, according to Lemma 1, there exists a FIR function $F(z^{-1})$ such that

$$\Re\{\psi(\rho_0)F(e^{-j\omega})\} > \gamma^{-1}|F(e^{-j\omega})W_q\Delta_q(\rho_0)| \quad \forall\omega \in \Omega \tag{27}$$

Therefore, there exists a higher order RST controller with $R = R(\rho_0)F$, $S = S(\rho_0)F$, and/or $T = T(\rho_0)F$ such that Statement (**b**) holds. ■

The above theorem is a necessary and sufficient condition for satisfying the $\mathcal{H}_\infty$ criterion for *one* sensitivity function. However, in typical control system applications, it is desired to shape several sensitivity functions simultaneously and impose multiple constraints on the weighted sensitivity functions. The following theorem ensures necessity and sufficiency of the $\mathcal{H}_\infty$ criterion when multiple sensitivity functions are considered:

Theorem 2. *Given the frequency response function $G(e^{-j\omega}) = N(e^{-j\omega})M^{-1}(e^{-j\omega})$ and the frequency response of bounded weighting filters $W_q(e^{-j\omega})$ for $\forall q \in \mathcal{Q}$, the following statements are equivalent:*

(a) *There exists an RST controller that stabilizes G and*

$$\sup_{\omega\in\Omega} |W_q\mathcal{S}_q(\rho)| < \gamma \quad \forall q \in \mathcal{Q} \tag{28}$$

(b) *There exists an RST controller such that*

$$\Re\{\psi(\rho)\} > \gamma^{-1}|W_q\Delta_q(\rho)| \quad \forall\omega \in \Omega \tag{29}$$

and for all $q \in \mathcal{Q}$.

Proof : (**b** $\Rightarrow$ **a**) The proof for this condition is equivalent to the proof presented in Theorem 1. By satisfying the constraint in (29) for all $q \in \mathcal{Q}$, the condition in (28) for each corresponding q is obtained.

(**a** $\Rightarrow$ **b**) Assume that $R(\rho_0)$, $S(\rho_0)$, and/or $T(\rho_0)$ satisfies Statement (**a**) but not Statement (**b**). Then, according to Lemma 1, there exist FIR transfer functions $F_q(z^{-1})$ such that

$$\Re\{F_q\psi(\rho_0) - \gamma^{-1}|F_qW_q\Delta_q(\rho_0)|\} > 0 \tag{30}$$

for all $\omega \in \Omega$ and for all $q \in \mathcal{Q}$. For Statement (**b**) to hold, there must exist a common F for all $q \in \mathcal{Q}$ such that $R = R(\rho_0)F$, $S = S(\rho_0)F$, and/or $T = T(\rho_0)F$.

[1]The inclusion of $T(\rho_0)$ depends on which sensitivity function $\mathcal{S}_q^0(\rho)$ is being considered

For a given frequency, the constraints in (28) will represent circles in the complex-plane that are centered exactly at $\psi(\rho_0)$ with varying radii (where the radii depend on each q). Let us define the following quantities at every $\omega \in \Omega$:

$$\begin{aligned}\mathscr{R}(e^{-j\omega},\rho_0) &= \{|W_1\Delta_1(e^{-j\omega},\rho_0)|,\ldots,|W_c\Delta_c(e^{-j\omega},\rho_0)|\}\\ r(e^{-j\omega},\rho_0) &= \gamma^{-1}\max_{q\in\mathcal{Q}}\mathscr{R}(e^{-j\omega},\rho_0)\end{aligned} \tag{31}$$

For any ω, the circle with radius $r(\rho_0)$ does not include the origin, and all of the other circles with smaller radii are enclosed in the circle with radius $r(\rho_0)$, i.e. :

$$\gamma^{-1}|W_q\Delta_q(e^{-j\omega},\rho_0)| \leq r(e^{-j\omega},\rho_0)$$

Therefore, for a given frequency, the complex number f_q which is used to rotate the circle associated with radius $r(e^{-j\omega},\rho_0)$ ensures that all of the circles with $\gamma^{-1}|W_q\Delta_q(e^{-j\omega},\rho_0)| \leq r(e^{-j\omega},\rho_0)$ are also rotated such that they all lie in the right-hand side of the imaginary axis. Therefore, there will always exist a common F that interpolates all f_q (different q in different frequencies) such that the conditions in (30) hold true for all $q \in \mathcal{Q}$. ■

B. Robust Design

With the proposed method, it is possible to design a fixed-structure controller which accounts for the uncertainties of a given FRF (as described in Section II-C). Given this additive uncertainty, a desired performance condition $\|W_q\mathcal{S}_q\|_\infty < \gamma$ will be satisfied for all models in the uncertain set (7) if $\|W_q\hat{\mathcal{S}}_q\|_\infty < \gamma$, where $\hat{\mathcal{S}}_q = \hat{\Delta}_q/\hat{\psi}(\rho)$ and $\hat{\psi}(\rho) = \hat{N}R(\rho) + \hat{M}S(\rho)$. For example, consider the nominal performance condition $\|W_3\hat{\mathcal{S}}_3\|_\infty < \gamma$ with $\hat{\Delta}_3(\rho) = \hat{M}S(\rho) + \hat{N}[R(\rho) - T(\rho)]$; as a worst case consideration, δ_m and δ_n can be selected to be equal to one in (7) (which ensures that the uncertainty in the entire disk is taken into account). By substituting the expressions in (7) into this condition, the following constraint can be devised:

$$\begin{aligned}\big|W_3\left[\psi(\rho) - NT(\rho) + S(\rho)|W_m|e^{j\theta_m} + C(\rho)|W_n|e^{j\theta_n}\right]\big| \\ < \gamma\big|\psi(\rho) + R(\rho)|W_n|e^{j\theta_n} + S(\rho)|W_m|e^{j\theta_m}\big| \\ \forall\omega\in\Omega, \forall\{\theta_n,\theta_m\} \in [0, 2\pi]\end{aligned} \tag{32}$$

where $C(\rho) = R(\rho) - T(\rho)$. For notation purposes, let us define $\psi'(\rho,\theta_n) := \psi(\rho) + R(\rho)|W_n|e^{j\theta_n}$. Then for a given $\{\omega,\theta_n,\theta_m\}$, (32) represents a circle centered at $\psi'(\rho,\theta_n) + S(\rho)|W_m|e^{j\theta_m}$ with a radius of

$$\begin{aligned}x_p(\rho,\theta_m,\theta_n) = \gamma^{-1}|W_3|\big|\psi'(\rho,\theta_n) + S(\rho)|W_m|e^{j\theta_m} \\ -T(\rho)[N + |W_n|e^{j\theta_n}]\big|\end{aligned} \tag{33}$$

According to Theorem 1, a necessary and sufficient condition for (32) can be constructed as follows:

$$\begin{aligned}x_p(\rho,\theta_m,\theta_n) < \Re\{\psi'(\rho,\theta_n) + S(\rho)|W_m|e^{j\theta_m}\} \\ \forall\omega\in\Omega, \forall\{\theta_m,\theta_n\} \in [0, 2\pi]\end{aligned} \tag{34}$$

By gridding in ω, θ_m and θ_n, then (33) becomes a convex constraint (with respect to ρ); however, gridding in all of these variables can be computationally expensive. For stable plants

(which is the case at CERN), $M = 1$ may be selected. Therefore, the disk uncertainty associated with M is $|W_m| = 0$. From (33) and (34), it can be observed that with $|W_m| = 0$, the dependency on θ_m is removed, and no gridding in θ_m is required. The necessary and sufficient condition then becomes

$$\begin{aligned} x_p(\rho, \theta_n) < \Re\{\psi'(\rho, \theta_n)\} \\ \forall \omega \in \Omega, \forall \theta_n \in [0, 2\pi] \end{aligned} \tag{35}$$

where

$$x_p(\rho, \theta_n) = \gamma^{-1}|W_3|\big|\psi'(\rho, \theta_n) - T(\rho)[N + |W_n|e^{j\theta_n}]\big| \tag{36}$$

In certain applications, gridding in two variables can still be computationally burdensome. Therefore, a sufficient condition for (32) can be devised as follows:

$$\sup_{\omega \in \Omega} \frac{|W_3|\big[|\psi(\rho) - NT(\rho)| + |C(\rho)W_n|\big]}{|\psi(\rho)| - |R(\rho)W_n|} < \gamma \tag{37}$$

With this condition, the dependency in θ_m and θ_n has been removed, and gridding in only one variable (i.e., ω) is required. Note that the above constraint is sufficient since

$$\begin{aligned} &|W_3|\big|\psi(\rho) - NT(\rho) + C(\rho)|W_n|e^{j\theta_n}\big| \\ &\leq |W_3|\big[|\psi(\rho) - NT(\rho)| + |C(\rho)W_n|\big] \\ &< \gamma\big[|\psi(\rho)| - |R(\rho)W_n|\big] \\ &\leq \gamma\big|\psi(\rho) + R(\rho)|W_n|e^{j\theta_n}\big| \end{aligned}$$

The condition in (37) can be represented as a disk in the complex plane which is centered at $\psi(\rho)$ and has radius

$$\begin{aligned} x_r(\rho) = \gamma^{-1}|W_3|\big[|\psi(\rho) - NT(\rho)| \\ +|C(\rho)W_n|\big] + |R(\rho)W_n| \end{aligned} \tag{38}$$

Therefore, a set of convex constraints (with respect to ρ) can be devised with the following condition:

$$x_r(\rho) < \Re\{\psi(\rho)\}, \quad \forall \omega \in \Omega \tag{39}$$

This constraint has the same structure as that of the sensitivity functions and so can readily be included in the optimization problem. Note that (37) introduces some conservatism; however, this conservatism can always be reduced by imposing (34) for unstable plants or (35) for stable plants.

C. Convex Optimization via Semi-Definite Programming

Suppose that it is desired to obtain $\mathcal{H}_\infty$ performance for a sensitivity function (i.e., minimize γ in $\|W_q\mathcal{S}_q\|_\infty < \gamma$). Then according to Theorem 2, one can formalize an optimization problem to obtain the admissible $R(\rho)$, $S(\rho)$, and/or $T(\rho)$ controllers as follows:

$$\begin{aligned} \underset{\rho}{\text{minimize}} \quad & \gamma \\ \text{subject to:} \quad & \gamma^{-1}|W_q\Delta_q| < \Re\{\psi(\rho)\} \\ & \forall \omega \in \Omega \quad ; \quad q \in \mathcal{Q} \end{aligned} \tag{40}$$

The optimization problem in (40) is quasi-convex since the objective function (γ) is being multiplied with the optimization parameters of the controller in the constraints. The classical solution is to implement a bisection algorithm in order to *convexify* the optimization problem. In this method, an iterative approach is implemented in order to obtain an asymptotically convergent solution.

Remark. *In the bisection method, an initial value is assigned for γ such that $\gamma_0 = 0.5(\gamma_{min} + \gamma_{max})$ to solve the optimization problem, where γ_{min} and γ_{max} are the minimum and maximum bounds set for γ. In an iterative algorithm, if the problem is feasible for γ_i, then $\gamma_{i+1} = 0.5(\gamma_{min} + \gamma_i)$, and the solution to the optimization problem in (40) is recalculated with γ_{i+1}. If the problem is infeasible for γ_i, then $\gamma_{i+1} = 0.5(\gamma_{max} + \gamma_i)$. This process is repeated until a solution is obtained within a given tolerance.*

The problem in (40) is known as a semi-infinite programming (SIP) problem since there are a finite number of optimization variables and an infinite number of constraints. To solve this problem, the optimization algorithm can be converted to a semi-definite programming (SDP) problem. A predefined frequency grid can be implemented in order to solve a finite number of constraints. This frequency grid can be predefined in a variety of manners (see [29], [17]).

IV. Power Converter Framework

Particle accelerators use power converters for many different applications. Some converters are used simply to convert energy in one form to another (to energize special devices); in other cases, power converters are used in a control structure to control particles trajectories (and other *optical* parameters of particle beams) within the accelerator system by modulating the magnetic field produced by specialized (electro-) magnets. These converters will be the focus of this paper. Particle beams usually require extremely precise magnetic fields; in certain cases, accuracy is also crucial for particle accelerators operation [30]. In most cases, the magnetic fields produced by the magnets cannot be measured in real-time. Therefore, the output current of the power converter (which is injected into the magnets) is used to control the trajectory of particles.

A. Power Converters for Particle Accelerators

The framework of the system discussed in this paper is part of the CERN Large Hadron Collider (LHC) Injector Upgrade Project [31], which was implemented to mitigate space-charge effects and to increase the beam brightness in order to fulfill the needs of the High Luminosity LHC. The Q-STRIP magnet (i.e., the load, which is constituted of two chains of quadrupole magnets) is used in this framework to control the particle trajectories via the power converter control system.

Power converters can be seen as systems comprised of three main subsystems: (*i*) a power source (usually a voltage source) (*ii*) a measuring system and (*iii*) a controller unit. The current is usually measured with a particularly accurate current transducer called a direct current-current transformer (DCCT) [32]. The current measurement signal is fed back to a digital controller unit which usually includes a high precision analog-to-digital converter that implements the digital control algorithm([30], [33]).

The general configuration of the CERN power converter control system is depicted in Fig.3. The control loop consists

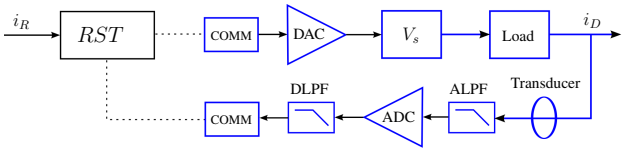

Fig. 3: Power converter control system

of a magnet (i.e., the load), a voltage source V_s, low-pass anti-aliasing analog and digital filters (ALPF, DLPF), a digital-to-analog converter (DAC), and an analog-to-digital converter (ADC). The DAC (optional) and ADCs are integrated in the control unit labeled as the function generator controller (FGC, [34]) whose main function is to execute the control algorithm; it also implements all the diagnostics and communication functions with higher layers of the control architecture up to the accelerators control rooms. The DLPF may also includes a decimator to reduce the sampling rate of the signal. The COMM block represents the delay associated with the communications link. The RST block represents the discrete-time controller that is used to control the magnet current i_D given a reference current i_R.

B. Experimental Test Setup

The experimental test setup consists of a CANCUN power converter, a dummy load and a proprietary software diagnostics tool:

- The CANCUN power converter is based on a full bridge phase shifted topology followed by a 4 quadrant switching stage to allow 4 quadrant operation. Fig. 4 shows a CANCUN converter that incorporates three main parts: i) Two high precision current sensors (DCCTs) which are able to measure DC or pulsed current at the required precision; ii) A voltage (or power) module; iii) A digital controller (FGC3) which implements the digital control loop together with CERN designed control and diagnostics electronics. The ratings of the CANCUN converter for the Q-STRIP application is $\pm 100\ A$ and $\pm 30\ V$.
- The dummy load is an RL load whose characteristics match those of the Q-STRIP magnets; however, the magnet used for the experiment has an inductance approximately 10% larger, which can be considered as a worst case for tracking performance evaluation.
- The software diagnostics tool interfaces with the main digital controller module, the FGC3 [34], and is able to acquire the relevant signals at a sampling rate of 10K samples per second. The acquired signals are the reference current and voltage, measured current, and voltage and current error. The length of the record is fixed to $1.2\ s$, which corresponds to 12000 samples.

V. Case Study Results

This case study is devoted to the CANCUN power converter control system, as described in the previous section. The objective is to control the output current i_D that is injected into the particle accelerator magnets in order to ensure proper particle trajectories. The profile of the reference current i_R

Fig. 4: CANCUN power converter.

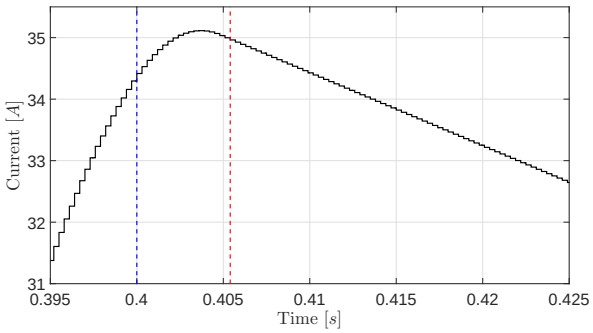

Fig. 5: The reference current associated with the QCF circuit configuration. The blue-dashed line indicates the time when the error must remain within ± 1000 ppm; the red-dashed line indicates the time when the error must remain within ± 100 ppm;

associated with the Q-STRIP magnet is shown in Fig. 5. For this application, the challenging task is to ensure the tracking performance; it is required that the error remains within ± 1000 ppm[2] during the fast transient and remains within ± 100 ppm during steady state. The proposed controller design method was used to synthesize an RST controller for this specific requirement. Experimental validation was performed by means of the test setup presented in IV-B.

The Q-STRIP magnet is represented as an RL circuit, and the dynamics of this circuit are dominant over the other components of the system. Thus a first order model with delay (i.e., $G_m(s) = e^{-sT_d}(L_m s + R_m)^{-1}$, where R_m is the circuit resistance, L_m is the circuit inductance, and T_d is the time delay) is appropriate to approximate the dynamics of the plant. For this case study, the model parameters are:

$$R_m = 164.3\,m\Omega; \quad L_m = 736.4\,\mu H; \quad T_d = 275.4\,\mu s$$

The model is then discretized using the zero-order-hold method and used to design an RST controller based on the model-reference control (MRC) strategy [22]. In this particular implementation of the strategy, the transfer function between

[2]The calculation for obtaining the error in ppm is performed by taking the raw data for the error and scaling it by a factor of $10^6/100$. The factor of 100 represents the nominal current (100 A) of the power converter for the Q-STRIP magnets.

the reference signal and output depends on the location of the single zero (which comes from modeling the fractional delay) of the system [35]. According to [22], if the fractional delay of the system is less than $0.5T_s$, then the zero of the system can be cancelled (which enables the tracking and regulation performances to be achieved without approximation). However, at CERN, this benchmark is modified such that the zero of the system is cancelled if the fractional delay is less than $0.4T_s$. In this case, the reference model is selected such that the transfer function from the reference input to the output will be a pure delay. However, if the fractional delay is greater than $0.4T_s$, then the corresponding zero cannot be cancelled, and the transfer function from the reference input to the output is represented as a fractional delay. The main difficulty of this approach is that the choice of the observer poles that lead to a good robustness margin is not trivial. The current practice at CERN is a trial-and-error approach to meet the control specifications. The main objective of this case study is to propose a systematic optimization based approach to compute the optimal controller parameters and guaranteeing robustness with respect to model uncertainties.

For this type of application, it is a challenging task to achieve tracking and a good robustness margin simultaneously. With the MRC method, the auxilary poles must be placed in an iterative fashion in order to achieve the desired modulus margin of 0.5. However, the method proposed in this paper does not need a parametric identification or any iterative tuning scheme. It is a straightforward systematic design methodology that takes also into account the frequency-domain uncertainties, which increases the robustness of the design process.

A. Frequency Response Function Measurement

A pseudo-random binary sequence (PRBS) signal was used as the input voltage reference of the open-loop system in order to capture the dynamics of the process. The PRBS is a deterministic signal which has characteristics similar to that of white noise and is usually used for system identification. From Fig. 3, the measurement process will capture the dynamics from the input of the DAC (with input voltage $v(t)$ representing the reference voltage of the voltage source) to the output of the DLPF (with output current $i(t)$ representing the measured current to be fed back to the RST controller).

Unfortunately, the FGC3 is limited by the amount of input samples that can be programmed to execute the PRBS signal (a maximum of 1023). Therefore, to maximize the quality of the measurement, a PRBS signal of length 511 (9-bits) with 2 periods was injected as the input of the open-loop process. Note that a PRBS of length 1023 (10-bits) with one period could also be used as the input; however, the output of such a reference will contain transients and must be considered as an aperiodic signal and thus increasing the truncation errors.

A total of 5 experiments were performed with the PRBS clock period $T_{cl} = 100\ \mu s$; the acquired periods (with transients removed in post-processing) could then be merged together. For a signal of length 511, the frequency resolution is limited to 255 points. A DC gain was added to this measurement in order to increase the resolution at lower

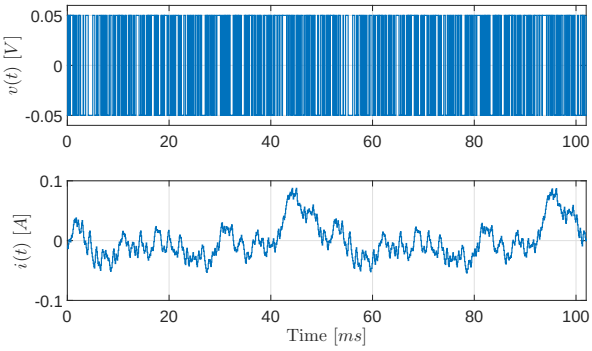

Fig. 6: PRBS signal used for the input voltage $v(t)$ of the open-loop system along with the resulting output current $i(t)$.

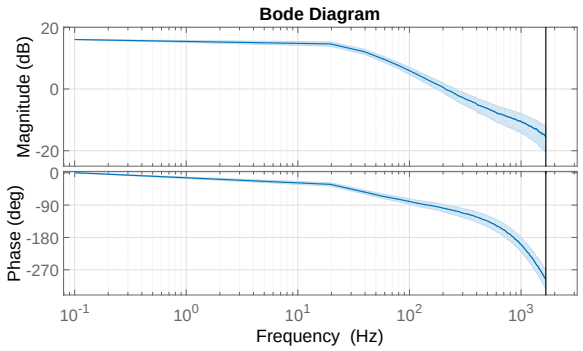

Fig. 7: Bode diagram of $G(e^{-j\omega})$ with additive uncertainty bounds for the corresponding frequency points.

frequencies (due to the low resolution resulting from the PRBS identification). This DC value was determined by simply applying a DC voltage $v(t) = V_{dc} = 1V$ and obtaining the value $i(t) = I_{dc}$. With 95% confidence, the uncertainty associated for this gain can be calculated as

$$|W_n(e^{-j\omega_0})| = 2\sigma_I/\sqrt{N_s} = 3.51 \times 10^{-4}$$

where ω_0 is chosen to be arbitrarily small ($\omega_0 = 0.2\pi$), $N_s = 12000$ is the length of the signal, and $\sigma_I = 0.0192\,A$ is the root-mean-square of the measurement noise. This specific value of the uncertainty is for the DC gain and not for all of the other corresponding frequencies. The uncertainties for the remaining frequencies were determined with (8). The PRBS input signal along with the resulting output response are shown in Fig. 6.

The FRF of the open-loop plant was then obtained as $G(e^{-j\omega}) = \mathcal{F}[i(t)]/\mathcal{F}[v(t)]$ (where the operator $\mathcal{F}$ signifies the Fourier Transform). From (8) and (9), the additive uncertainty associated with each frequency can be computed. Fig. 7 displays a Bode diagram of $G(e^{-j\omega})$ with the corresponding uncertainty bounds.

B. Controller Stability

Computation of an unstable controller should generally be avoided [22]. The logic behind this assertion has to do with the practical implications involved with a feedback control system.

Suppose that the plant $G(z^{-1}) = N(z^{-1})M^{-1}(z^{-1})$ is analytic outside the unit circle. For the RST structure, it is evident that if the polynomial $S(z^{-1}, \rho)$ possesses zeros outside the unit circle, then the open-loop system will become unstable (assuming no zero-pole cancellations occur with $R(z^{-1}, \rho)$ and $S(z^{-1}, \rho)$). In order to avoid this impairment, it is required to impose a constraint such that the polynomial $S(z^{-1}, \rho)$ possesses zeroes inside the unit circle. This rationalization leads to the following lemma:

Lemma 2. *Suppose that $S(z^{-1}, \rho)$ is parameterized as in (11). Then a sufficient (convex) condition to ensure that the zeros of $S(z^{-1}, \rho)$ remain inside the unit circle is*

$$\Re\{S(\rho)\} > 0; \quad \forall \omega \in \Omega \tag{41}$$

Proof: First note that a strictly positive real transfer function (and its inverse) is stable. $\Re\{S(\rho)\} > 0$ implies that the Nyquist diagram of $S(\rho)$ will not encircle the origin. Therefore, $S^{-1}(\rho)$ will not encircle the origin, and $S(\rho)$ is stable. ■

C. Weighting Filter Design

The $\mathcal{H}_\infty$ criterion in (16) is a very powerful design tool, as it provides the capability to shape any sensitivity function $\mathcal{S}_q$ based on the specifications set by a weighting filter. However, in certain design schemes at CERN, it may be desired to bound a sensitivity function to a particular value. For example, it may be desired to simply impose a lower-bound on the modulus margin in order to obtain the intended robust performance of a system. The modulus margin is defined as the minimum distance between the critical point $(-1 + j0)$ and the Nyquist plot of the open loop transfer function, and can be expressed as

$$M_m = \|\mathcal{S}_1\|_\infty^{-1} \tag{42}$$

In general, it is desired to obtain a minimum value of the modulus margin in order to ensure a sufficiently robust system. Let m_d denote the minimum value of the desired modulus margin such that $M_m > m_d$. According to [22], typical values for a good modulus margin are $M_m \geq 0.5$ $(-6\ dB)$ (which ensures a gain margin of at least 6 dB and a phase margin of at least 29°). A constraint for ensuring a minimum value of the modulus margin can be constructed as follows:

$$\|m_d \mathcal{S}_1\|_\infty < 1 \tag{43}$$

This constraint is a special case of the $\mathcal{H}_\infty$ constraints with $W_1(e^{-j\omega}) = m_d$ and can be convexified using the results of Theorem 2.

For this particular case study, it is desired to obtain the best tracking performance (i.e., by minimizing γ in $\|W_3\mathcal{S}_3\|_\infty < \gamma$) while ensuring reasonable stability margins. The weighting filter W_3 is chosen based on the fact that $\mathcal{S}_2^d + \mathcal{S}_3^d = 1$, where $\mathcal{S}_3^d$ is the desired error sensitivity function and $\mathcal{S}_2^d$ is the desired complementary sensitivity function (i.e., the closed-loop transfer function). $\mathcal{S}_2^d$ was chosen as a standard second order transfer function with the given form:

$$\mathcal{S}_2^d(s) = \frac{\omega_d^2}{s^2 + 2\zeta\omega_d s + \omega_d^2} \tag{44}$$

where ζ is the damping factor and

$$\omega_d = \frac{2\pi f_d}{\sqrt{1 - 2\zeta^2 + \sqrt{2 - 4\zeta^2 + 4\zeta^4}}}$$

where f_d is the desired closed-loop bandwidth. Note that it is possible to consider a continuous-time transfer function for this specification since the proposed method implements a frequency-domain approach. Since $\mathcal{S}_2^d = 1 - \mathcal{S}_3^d$, an appropriate filter for the error sensitivity function can be devised as

$$W_3(s) = \frac{s^2 + 2\zeta\omega_d s + \omega_d^2}{s(s + 2\zeta\omega_d)} \tag{45}$$

Due to the fact that $W_3(j\omega_k)$ is evaluated at a finite number of frequency points with $\omega_0 \neq 0$, then the integrator in W_3 does not pose problems with boundedness.

A simulation was performed to determine the bandwidth that is required in order to satisfy the desired error specifications. At CERN, the error is calculated with respect to a delayed reference input (i.e., $e(t) = r(t - \tau) - y(t)$). By assuming that the closed-loop response behaves as $\mathcal{S}_2^d$, the bandwidth f_d can be selected such that the error between the delayed reference input and output is within ± 100 ppm. For this second order response, this delay was analytically derived as $\tau = 2\zeta/\omega_d$. It was determined that $f_d = 300\ Hz$ with $\zeta = 0.8$ satisfies these requirements.

D. RST Controller Synthesis

The voltage applied to the magnet by the voltage source and the relative current are both sampled at 10 kHz while the control loop is run 3 times slower (i.e., $f_s = 3.333$ kHz and $T_s = 300$ μs, where f_s and T_s are denoted as the sampling frequency and sampling time of the control loop, respectively). Since the plant is stable, then a possible selection for the coprime factors is $N(e^{-j\omega}) = G(e^{-j\omega})$ and $M(e^{-j\omega}) = 1$. For proper implementation within the proprietary power converter control software, it is required that all the open-loop poles remain on or within the unit circle, i.e. the controller should be marginally stable. This implies that the zeroes of $S(\rho)$ must lie on or within the unit circle. Since the reference current is close to a ramp signal, to achieve adequate performance, $S(z^{-1}, \rho)$ must incorporate a double integrator: $S(z^{-1}, \rho) = (1 - z^{-1})^2 S^\star(z^{-1}, \rho)$. With the FRF measured by means of the PRBS excitation, the constraints for the convex optimization problem are formulated. With a minimum value of $m_d = 0.5$ set for the modulus margin, the following optimization problem must be solved:

$$\begin{aligned} \underset{\rho \in \mathbb{R}}{\text{minimize}} \quad & \gamma \\ \text{subject to:} \quad & \Re\{\psi(e^{-j\omega_k}, \rho)\} > x_r(e^{-j\omega_k}, \rho) \\ & \Re\{\psi(e^{-j\omega_k}, \rho)\} > m_d |S(e^{-j\omega_k}, \rho)| \\ & \Re\{S^\star(e^{-j\omega_k}, \rho)\} > 0 \\ & \text{for } k = 0, \ldots, \eta \end{aligned} \tag{46}$$

where

$$\psi(e^{-j\omega_k}, \rho) = S(e^{-j\omega_k}, \rho) + N(e^{-j\omega_k}) R(e^{-j\omega_k}, \rho)$$

TABLE I: Parameters resulting from the bisection algorithm.

Parameter	*Value*	*Unit*
$\gamma_{\max}$	2.5	-
$\gamma_{\min}$	0	-
γ_{tol}	10^{-6}	-
γ_{opt}	1.202	-
Optimization time[3]	61.3	s

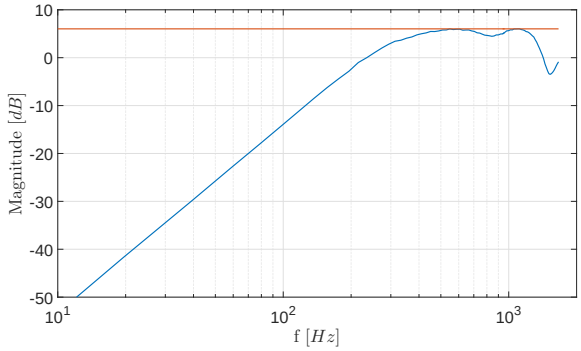

Fig. 8: FRF of the output sensitivity function $\mathcal{S}_1$ (solid-blue line) and the bound for the modulus margin.

and $x_r(e^{-j\omega_k}, \rho)$ is defined as in (38). The first inequality in (46) ensures that $\mathcal{H}_\infty$ nominal performance is achieved for the RST structure whilst considering the frequency dependent uncertainties. The second inequality ensures that the modulus margin is at least 0.5. With the additional low-frequency measurement at ω_0, there will be a total of 256 frequency points ($\eta = 255$, $\omega_k \in (0, \pi f_s]\ \forall k$).

E. Optimization Results

The SDPT3 open-source optimization package was used in conjunction with Matlab to perform the bisection algorithm [36]. The solution to the optimization problem in (46) leads to a 9-th order stable controller that achieves the desired performance. The main parameters of the bisection algorithm are tabulated in Table. I.

The obtained output sensitivity function $|\mathcal{S}_1|$ is depicted in Fig. 8. It can be observed that this sensitivity function is indeed bounded by the modulus margin constraint and that a modulus margin of 0.5 is obtained.

For the reference current applied to this system, the error between the reference and the output current is determined by shifting the reference current such that a minimum peak error is achieved; this will be shown in the next section.

F. Experimental Validation and Comparison

The reference and measured currents were acquired for the profile required by a specific Q-STRIP magnet (Fig. 5). As stated in section V-C, the error is calculated with respect to a delayed reference input (i.e., $e(t) = r(t-\tau) - y(t)$). For comparison purposes, the value of τ was found by shifting the reference profile such that the minimum peak error was achieved. A total of 10 experiments were performed; the error for both the model-based and data-driven based designs (with the associated error-bars showing the minimum and maximum errors at each sampling instant) are shown in Fig. 9. It can be observed that both designs are comfortably within the ± 1000 ppm fast-transient requirement and within the ± 100 ppm steady-state requirement. Indeed, both controllers achieve ± 100 ppm even during the fast-transients. However, the proposed method ensures that all of the design requirements are met while eliminating the iterative process of attaining robust performance from the model-based methodology. Therefore, the proposed data-driven method proves to be superior as it achieves all of the design objectives in a single attempt.

[3]This optimization time was calculated based on a computer having the following hardware specifications: Intel-Core i7, 3.4 GHz CPU, 8 GB RAM. The optimization algorithm was run using MATLAB version 8.6.0.267246 (R2015b) on a Windows 7 platform (64-bit).

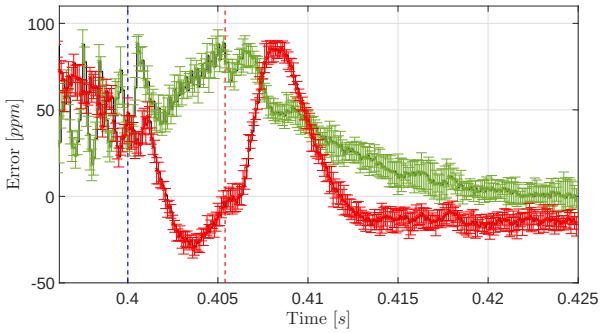

Fig. 9: Comparison between the error resulting from the model-based design (solid-black line with red error-bars) and the error resulting with the proposed method (solid-black line with green error-bars).

VI. Conclusion

A new data-driven method for computing a robust controller that attains $\mathcal{H}_\infty$ performance has been presented. A frequency-domain approach has been used in order to avoid the problem of unmodeled dynamics associated with parametric models. The necessary and sufficient conditions for the existence of RST controllers with multiple $\mathcal{H}_\infty$ performance have been developed in terms of a set of convex constraints. Constraints have been devised in order to design a controller which considers frequency dependent uncertainties, ensures a minimum value for the modulus margin, and to assure the controller stability. This method has been applied to a power converter control system which uses an RST controller structure and is used for experimental purposes at CERN. In the case study presented in this paper, it has been shown that the proposed data-driven method offers an optimization-based systematic approach that leads to low-order RST controllers meeting the challenging specification for particle trajectory tracking. With the proposed methodology, the process of obtaining a model and iteratively tuning the desired closed-loop bandwidth to attain the proper stability margins is eliminated whilst achieving the desired tracking performance.

REFERENCES

[1] Z.-S. Hou and Z. Wang, "From model-based control to data-driven control: Survey, classification and perspective," *Information Sciences*, vol. 235, pp. 3–35, 2013.

[2] A. S. Bazanella, L. Campestrini, and D. Eckhard, *Data-driven Controller Design: The H_2 Approach*. Springer, 2012.

[3] I. D. Landau, R. Lozano, M. M'Saad, and A. Karimi, *Adaptive Control: Algorithms, Analysis and Applications*. London: Springer-Verlag, 2011.

[4] Z. Hou and S. Jin, *Model free adaptive control: theory and applications*. CRC press, 2013.

[5] M. G. Safonov and T. C. Tsao, "The unfalsified control concept and learning," *IEEE Trans. on Automatic Control*, vol. 42, no. 6, 1997.

[6] H. Hjalmarsson, "Iterative feedback tuning - an overview," *Int. Journal of Adaptive Control and Signal Processing*, vol. 16, pp. 373–395, 2002.

[7] A. Karimi, L. Mišković, and D. Bonvin, "Convergence analysis of an iterative correlation-based controller tuning method," in *15th IFAC World Congress, Barcelona, Spain*, July 2002.

[8] M. C. Campi, A. Lecchini, and S. M. Savaresi, "Virtual reference feedback tuning: A direct method for the design of feedback controllers," *Automatica*, vol. 38, pp. 1337–1346, 2002.

[9] A. Karimi, K. van Heusden, and D. Bonvin, "Non-iterative data-driven controller tuning using the correlation approach," in *European Control Conference*, Kos, Greece, 2007, pp. 5189–5195.

[10] R. Hoogendijk, A. J. Den Hamer, G. Angelis, R. van de Molengraft, and M. Steinbuch, "Frequency response data based optimal control using the data based symmetric root locus," in *IEEE Int. Conference on Control Applications*, Yokohama, Japan, 2010, pp. 257–262.

[11] S. Khadraoui, H. Nounou, M. Nounou, A. Datta, and S. Bhattacharyya, "Robust control design method for uncertain system using a set of measurements," in *American Control Conference (ACC), 2013*, 2013, pp. 4325–4330.

[12] ——, "A control design method for unknown systems using frequency domain data," in *Control Conference (ASCC), 2013 9th Asian*. IEEE, 2013, pp. 1–6.

[13] A. J. Den Hamer, S. Weiland, and M. Steinbuch, "Model-free norm-based fixed structure controller synthesis," in *48th IEEE Conference on Decision and Control*, Shanghai, China, 2009, pp. 4030–4035.

[14] A. Karimi and G. Galdos, "Fixed-order H_∞ controller design for nonparametric models by convex optimization," *Automatica*, vol. 46, no. 8, pp. 1388–1394, 2010.

[15] M. Saeki, M. Ogawa, and N. Wada, "Low-order H_∞ controller design on the frequency domain by partial optimization," *International Journal of Robust and Nonlinear Control*, vol. 20, no. 3, pp. 323–333, 2010.

[16] A. Karimi and Z. Emedi, "H_∞ gain-scheduled controller design for rejection of time-varying narrow-band disturbances applied to a benchmark problem," *European Journal of Control*, vol. 19, no. 4, pp. 279–288, 2013.

[17] G. Galdos, A. Karimi, and R. Longchamp, "H_∞ controller design for spectral MIMO models by convex optimization," *Journal of Process Control*, vol. 20, no. 10, pp. 1175 – 1182, 2010.

[18] A. Karimi, "Frequency-domain robust control toolbox," in *52nd IEEE Conference in Decision and Control*, 2013, pp. 3744 – 3749.

[19] M. Hast, K. J. Aström, B. Bernhardsson, and S. Boyd, "PID design by convex-concave optimization," in *European Control Conference*, Zurich, Switzerland, 2013, pp. 4460–4465.

[20] S. Boyd, M. Hast, and K. J. Åström, "MIMO PID tuning via iterated LMI restriction," *International Journal of Robust and Nonlinear Control*, vol. 26, no. 8, pp. 1718–1731, 2016.

[21] A. Karimi, A. Nicoletti, and Y. Zhu, "Robust H_∞ controller design using frequency-domain data via convex optimization," *available online in International Journal of Robust and Nonlinear Control*, 2016.

[22] I. D. Landau and G. Zito, *Digital control systems: design, identification and implementation*. Springer, 2006.

[23] G. Galdos, A. Karimi, and R. Longchamp, "RST controller design by convex optimization using frequency-domain data," in *Proceedings of the 18th IFAC World Congress*, Milan, Italy, 2011.

[24] A. Nicoletti, Z. Emedi, and A. Karimi, "A data-driven approach in designing RST controllers with H_∞ performance via convex optimization," in *54th IEEE Conference on Decision and Control (CDC)*, Osaka, Japan, 2015, pp. 6650–6655.

[25] L. Ljung, *System Identification - Theory for the User*, 2nd ed. NJ, USA: Prentice Hall, 1999.

[26] K. Zhou and J. C. Doyle, *Essentials of robust control*. N.Y.: Prentice-Hall, 1998.

[27] C. J. Doyle, B. A. Francis, and A. R. Tannenbaum, *Feedback Control Theory*. New York: Mc Millan, 1992.

[28] A. Rantzer and A. Megretski, "Convex parameterization of robustly stabilizing controllers," *IEEE Trans. on Automatic Control*, vol. 39, no. 9, pp. 1802–1808, September 1994.

[29] P. Seiler, B. Vanek, J. Bokor, and G. J. Balas, "Robust H_∞ filter design using frequency gridding," in *American Control Conference (ACC), 2011*. IEEE, 2011, pp. 1801–1806.

[30] H. Thiesen, S. Page, V. Montabonnet, Q. King, G. Hudson, D. Nisbet, and M. Cerqueira Bastos, "High precision current control for the LHC main power converters," in *International Particle Accelerator Conference (IPAC)*, 2010.

[31] W. Bartmann, K. Hanke, J. Abelleira, and M. Kowalska, "Upgrades of the CERN PS booster ejection lines," No. CERN-ACC-2014-0202, Tech. Rep., 2014.

[32] Q. King, "The all-digital approach to LHC power converter current control," in *Accelerator and Large Experimental Physics Control Systems*, vol. 1, 2001, pp. 453–455.

[33] M. Bastos, G. Fernqvist, A. Cantone, and Q. King, "Developments in high-precision aspects of power converter control for LHC," No. CERN-LHC-PROJECT-Report-1044, Tech. Rep., 2007.

[34] D. Calcoen, Q. King, and P. Semanaz, "Evolution of the CERN power converter function generator/controller for operation in fast cycling accelerators," in *International Conference on Accelerator and Large Experimental Control Systems (ICALEPCS)*, Grenoble, France, 2011.

[35] Q. King, A. Nicoletti, R. Murillo Garcia, M. Magrans De Abril, K. T. Lebioda, and M. Martino, "CCLIBS: The CERN power converter control libraries," in *International Conference on Accelerator and Large Experimental Physics Control Systems*, Melbourne, Australia, 2015.

[36] K. C. Toh, M. J. Todd, and R. H. Tutuncu, "SDPT3: a MATLAB software package for semidefinite programming," *Optimization Methods and Software*, vol. 11, pp. 545–581, 1999.